crystals

MDPI

Article

Reactively Synthesized Porous Ti_3SiC_2 Compound and Its Mechanical Properties with Different Apertures

Yao Jiang [1,*], Xinli Liu [2], Haiyan Gao [1] and Yuehui He [1]

[1] State Key Laboratory of Powder Metallurgy, Central South University, Changsha 410083, China; gaohy@csu.edu.cn (H.G.); yuehui@csu.edu.cn (Y.H.)

[2] School of Materials Science and Engineering, Central South University, Changsha 410083, China; liuxinli@csu.edu.cn

* Correspondence: jiangyao@csu.edu.cn

Received: 14 January 2020; Accepted: 1 February 2020; Published: 2 February 2020

Abstract: Reactively synthesized porous Ti_3SiC_2 with different pore sizes was prepared using TiH_2, Si and graphite powders as starting materials. The effect of pore size on the flexural stress–strain relationship, bending strength and flexural elastic modulus were investigated. The results show that the synthesized porous Ti_3SiC_2 intermetallic compounds have a characteristic of a high-purity MAX phase with typical laminate microstructure. When the average pore size decreases from 21.8 to 2.1 μm, the volume content of Ti_3SiC_2 phase ranges from 96.9% to 99.6%, and the porosity is in the range of 49.9% to 54.1%. The flexural stress–strain curves of porous Ti_3SiC_2 show a characteristic of two stages of elastic deformation and fracture. The flexural modulus is in the range of 13 to 70 GPa, which increases rapidly with further decrease of the pore size. A relation similar to the Hall–Petch equation between the mechanical property and the pore size was investigated for the porous material.

Keywords: Ti_3SiC_2; intermetallic compound; porous material; mechanical property; pore size; elastic modulus

1. Introduction

Porous Ti_3SiC_2 [1–5], as a new type of porous intermetallic compound with MAX phase, has the performance advantages of porous metals and ceramics, such as excellent environmental corrosion resistivity [1], high temperature stability [2] as well as good thermal shock resistance and machining performance [3]. In addition, porous Ti_3SiC_2 prepared by reactive synthesis of elemental powders [6–8] also shows a good open-pore structure and pore-structure stability [1,2].

Compared with dense material, the mechanical strength of porous material decreases significantly [9–11]. The mechanical model [8,12], microstructure [8] and the effect of porosity on mechanical properties [12,13] of porous Ti_3SiC_2 have been investigated, which is classified as a kinking nonlinear elastic solid [14,15]. The strength and stiffness of porous Ti_3SiC_2 decrease with increasing the porosity [12]. In the case of porous MAX phases prepared with space holder with the size of several hundred microns [4,5,13], it was found that the porosity and the pore type were the main factors influencing the elastic properties [13]. On the other hand, porous Ti_3SiC_2, due to its unique pore structure and material properties, can be well applied in biological separation [16], chemical filtration and hydrometallurgy [1], etc., where the mechanical properties of porous materials should meet the requirements of the working conditions [3]. The pore size is an important pore structure parameter determining the filtration accuracy, and its influence on mechanical properties is an important design basis for porous materials in the filtration application. To the best of our knowledge, investigations on the effect of pore size of porous Ti_3SiC_2 on its strength and stiffness have not been reported so far.

Currently, the relationship between porosity and strength of porous materials can be simulated by the Barsen equation [17]. The Hall–Petch equation can be used to reveal the relation between the strength or hardness and the grain size of single phase material [18–20] or composite material [21–23]. In this work, a series of porous Ti_3SiC_2 compounds with different pore sizes and approximately the same porosities and phase purities were prepared by the reactive synthesis of elemental powders through a pressure less sintering process. The Hall–Petch relationship between the pore size and the bending strength was studied, and the effect of pore size on the flexural modulus of porous Ti_3SiC_2 was discussed.

2. Experimental Procedure

Porous Ti_3SiC_2 compounds were prepared using commercially available TiH_2, Si and graphite powders as the starting materials by a pressure less sintering process [1]. TiH_2 powder can be prepared by hydrogenation of titanium sponge and subsequent mechanical pulverization process [24]. The median diameter of TiH_2 powder is in the range of 10 to 180 μm, which was utilized to fabricate porous material with different pore sizes. The median diameters of Si and graphite powders are in the ranges of 10–15 μm and 5–10 μm, respectively. The purities of all the used powders were above 99.0 wt.%, and were mixed according to the atomic ratio of Ti, Si, and C of 3:1.2:2. An excess of 20% Si was added to compensate for its high temperature volatilization loss [1,3]. Analytically pure stearic acid was used as forming agent and lubricant. Cold forming procedure was carried out by means of uniaxial die pressing with the pressure of 100 MPa. The prepared compacts are cuboids with dimensions of length, width and thickness of 30 mm, 6–7 mm and 2–3 mm, respectively. A multi-stage heating process under vacuum was utilized for the sintering of compacts [3]. The sintering procedure diagram is shown in Figure 1. The low-temperature sintering process at 350 °C is designed to decompose and remove the organic additives from the compacts, which is followed by a heating stage at 650 °C to dehydrogenate TiH_2. At the intermediate sintering stage at 1000 °C, the binary intermediate phases including TiC and Ti_5Si_3 are gradually formed through the solid phase diffusion [3,6], which is conducive to the subsequent synthesis of Ti_3SiC_2 [3]. The final sintering temperature is 1350 °C for 3 h with the vacuum pressure of 10^{-1}–10^{-3} Pa. The heating rate is controlled at 5–10 °C/min. After the pressure less sintering, the compacts are cooled with the furnace.

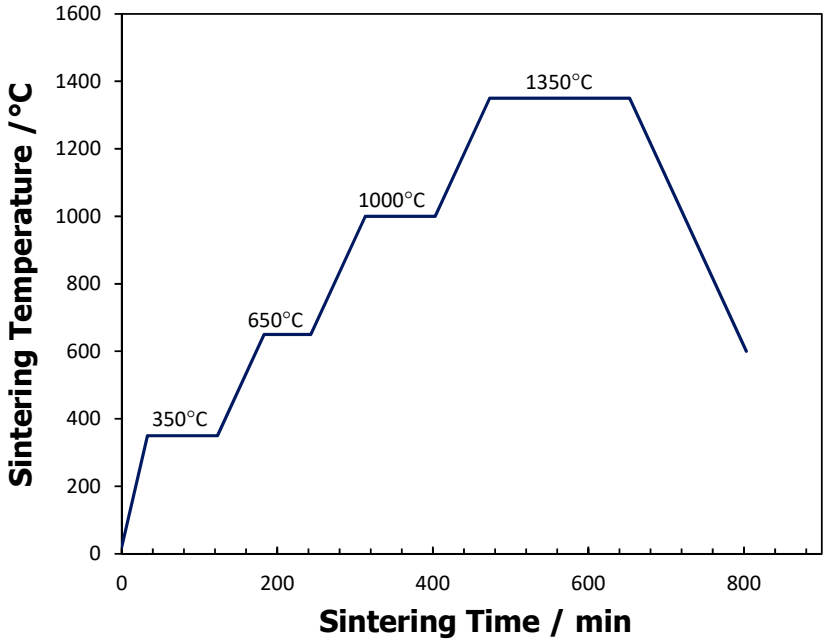

Figure 1. Temperature-time diagram for the sintering procedure of cold pressed compacts.

The phase compositions of the compacts after sintering at 1350 °C for 3 h were analyzed by X-ray diffraction (XRD: Dmax 2500VB, Tokyo, Japan) with a Cu Kα source at room temperature. The corresponding XRD data processing and analysis was carried out by Jade5 software (MDI, California, USA). The mechanical properties and the relation between flexural stress and strain of porous Ti_3SiC_2 were measured according to the three point flexural test by an electric servo-hydraulic material test system (Instron3369, Instron Ltd., High Wycombe, UK). The sintered compacts with the rectangular section mentioned above were used as the samples for the bending strength test, in which the span and the displacement rate are 25 mm and 0.02 mm/min, respectively. The mechanical strengths are the average of the three replicates used. The pore size was determined by the bubble point method (FBP-III) [6]. The open and overall porosities were calculated through the pycnometry method.

3. Results and Discussion

The XRD patterns of porous Ti_3SiC_2 with three different average pore sizes are shown in Figure 2. The phases of these porous materials are composed of Ti_3SiC_2 phase (a = 3.062 Å and c = 17.637 Å, Space Group P63/mmc, PDF 40-1132) and a small amount of TiC impurity phase (a = 4.327 Å, Space Group Fm-3m, PDF 65-0242). According to the standard additive method [25], the Ti_3SiC_2 phase volume contents of the porous compounds with average pore sizes of 2.1, 12.9 and 21.8 μm have been calculated to be 99.6%, 98.8% and 96.9%, respectively, showing a high-purity characteristic. The MAX phase content of porous Ti_3SiC_2 increases to a certain extent as the pore size reduces. The phase composition of porous Ti_3SiC_2 compounds prepared by reactive synthesis has been investigated to be influenced by the raw material type [1], the synthesis parameters [3], the material composition and alloying elements [7] and the material granularity [16]. The addition of TiH_2 was proved to improve the phase purity of the synthesized Ti_3SiC_2 MAX phase, which was attributed to the low oxygen content and high reactivity of elemental Ti generated from the dehydrogenation of TiH_2 [1,3].

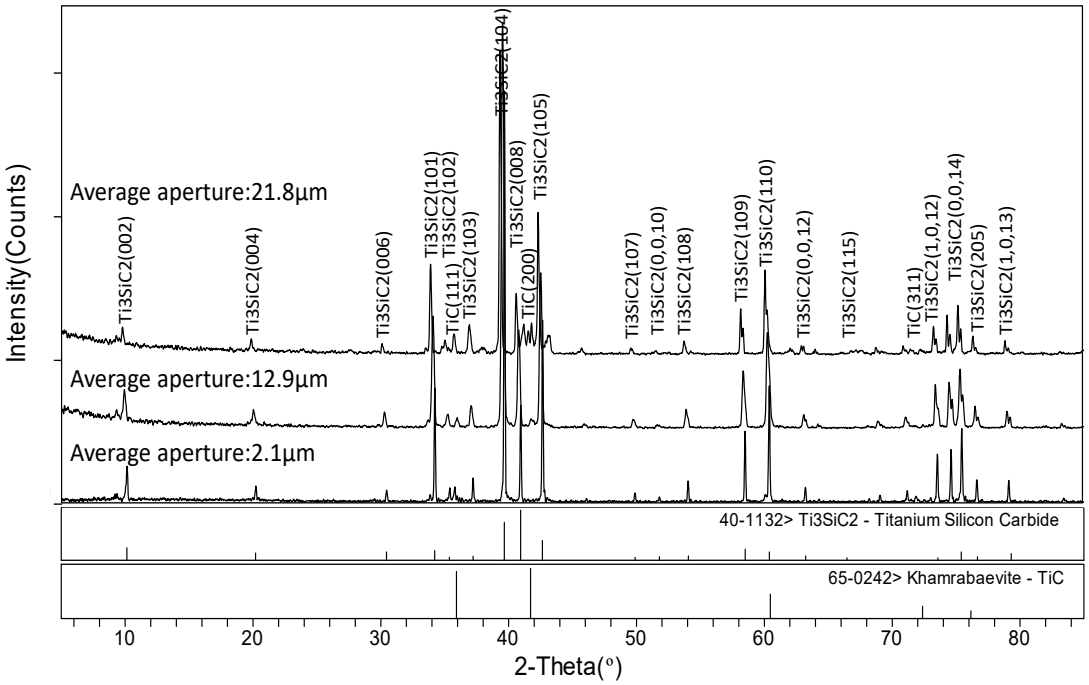

Figure 2. X-ray diffraction (XRD) patterns of porous Ti_3SiC_2 with different average pore sizes.

In the preparation process of porous Ti_3SiC_2 by the reactive synthesis of TiH_2, Si and graphite, the pore size of the resultant porous material has a strict linear relation with the powder particle size of TiH_2, and the porosity is kept essentially constant when the pore size changes [6]. Therefore, the pore size of porous Ti_3SiC_2 can be adjusted by changing the powder size of TiH_2. In fact, the synthesized

porous Ti_3SiC_2 in this work has the average pore size in the range of 2.1–21.8 μm with the open and overall porosities in the ranges of 44.6%–48.5% and 49.9%–54.1%, respectively. The decrease of pore size means the increase of specific surface area of the reactant under the condition that porosity is basically constant, which helps to enhance the surface diffusion during the synthesis process.

Figure 3 reveals the pore structure morphology and the lamellar microstructure of porous Ti_3SiC_2. The synthesized Ti_3SiC_2 compound has the characteristics of rich porous structure and high specific surface area, as shown in Figure 3a and b with the average apertures of 6.2 μm and 3.0 μm, respectively. A large number of interconnected pores are generated in the sintered compact with the aperture at the micron level. A few coarse pores exist locally, which is related to the original particle clearance in the compacts [7]. The prepared Ti_3SiC_2 phase skeleton generally has a smooth surface, which is conducive to the permeability of the porous material. Further observations reveal that the Ti_3SiC_2 grains exhibit obvious lamellar characteristic with the grain size in the range of several microns (Figure 3c), which is a typical microstructure feature of the reactively synthesized MAX phase [1–3].

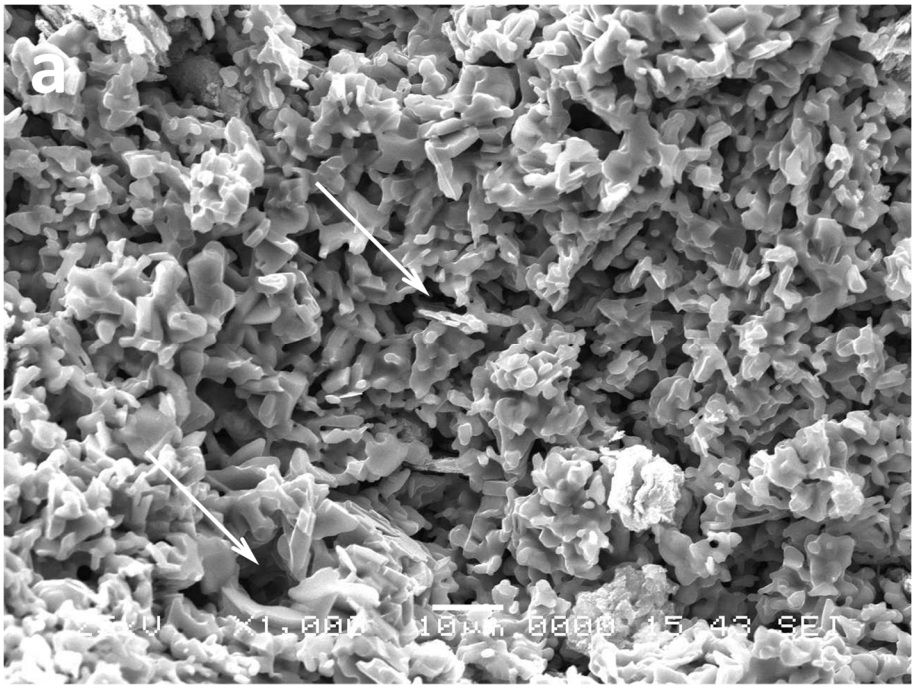

Figure 3. *Cont.*

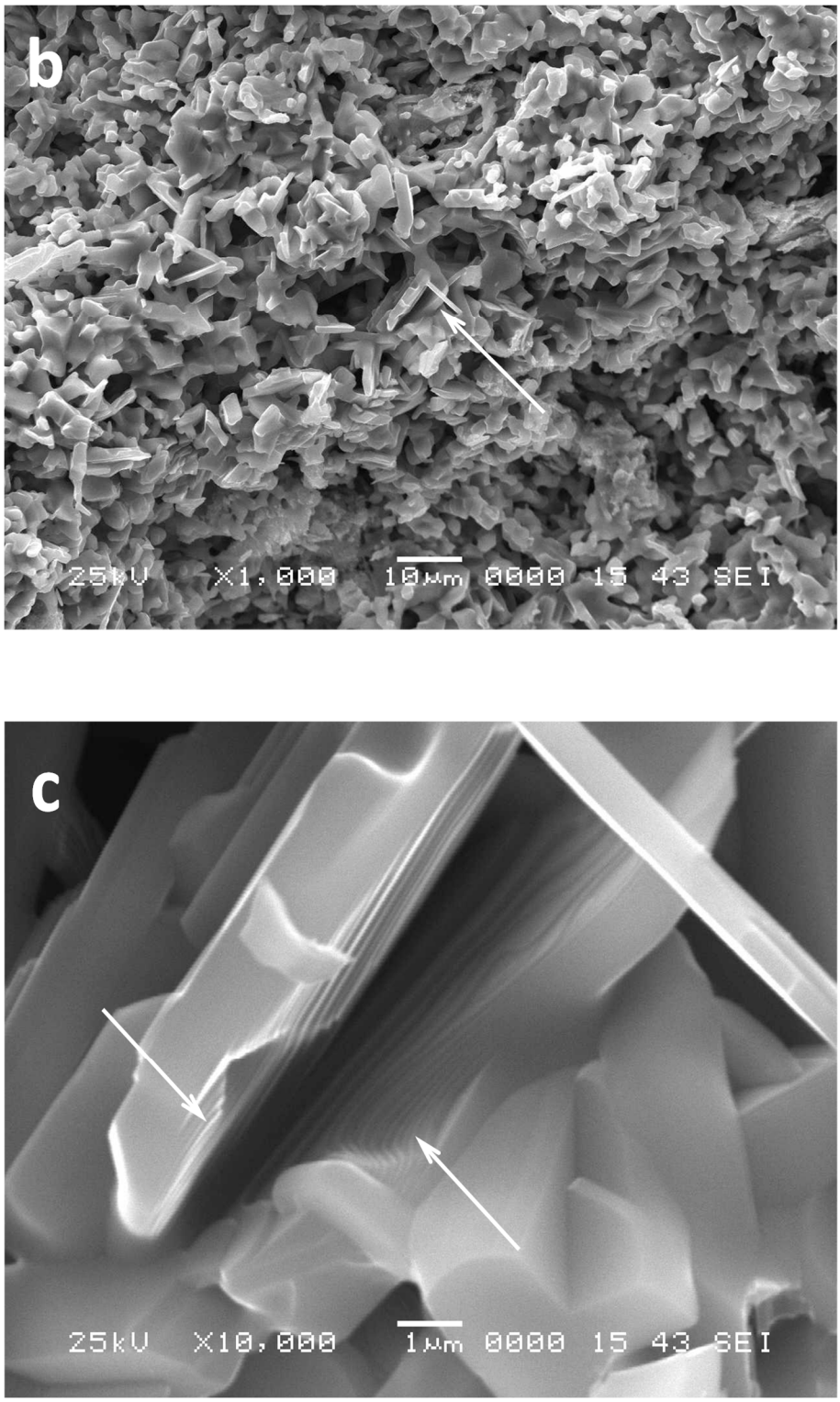

Figure 3. SEM images of the pore structure morphology of the sintered compacts with the average apertures of 6.2 μm (**a**) and 3.0 μm (**b**) and the lamellar microstructure of the synthesized porous Ti_3SiC_2 (**c**).

Figure 4 shows the relation between the flexural stress and strain for porous Ti_3SiC_2 with different average pore sizes. The variation rate of flexural stress with strain increases with decreasing the pore size. All the stress–strain curves show a typical elastic deformation stage directly followed by a fracture stage. However, the flexural stress increases nonlinearly with increasing strain, which is

mainly attributed to the deformation of the MAX phase as a kinking nonlinear elastic solid through the formation of regular and incipient kink bands [12].

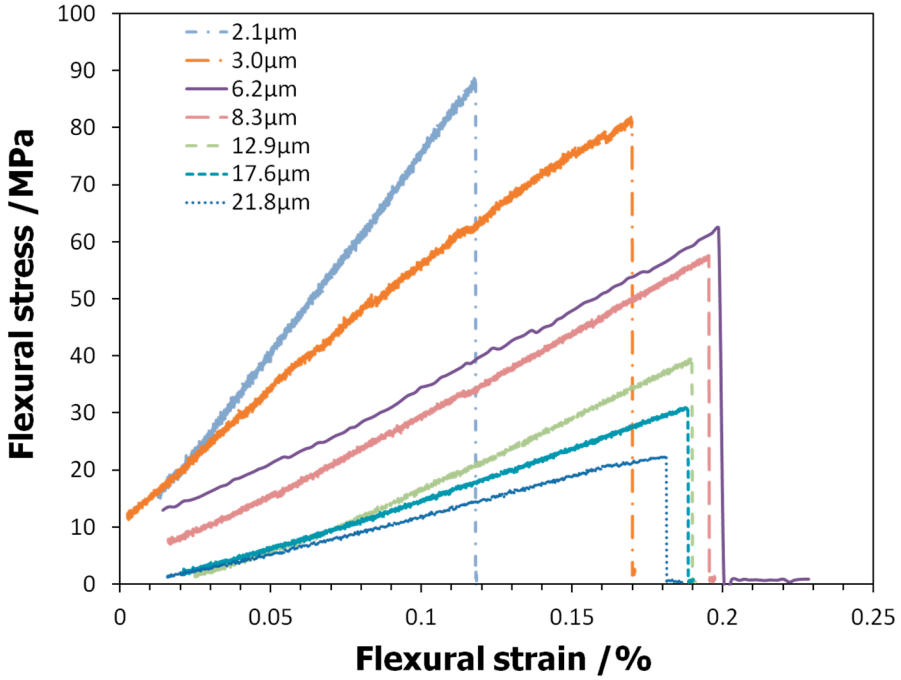

Figure 4. Flexural stress–strain curves of porous Ti_3SiC_2 with different average pore sizes.

Figure 5 shows the relation between the bending strength and the average pore size of porous Ti_3SiC_2. The bending strength increases in a nonlinear manner with decreasing the average pore size (Figure 5a). As the aperture decreases from 21.8 to 2.1 μm, the bending strength increases from 22 to 89 MPa. Through data fitting, the relationship between them is as follows:

$$\sigma = k \cdot d^{-\lambda} \quad (1)$$

where σ and d are the bending strength (MPa) and the average pore size (μm) of the porous material, respectively. k and λ are the constants with the values of 154.04 and 0.56, respectively. The determination coefficient R^2 of the fitting relation equation is 0.92. Given λ is close to 0.5, further relationship between σ and $d^{-0.5}$ is investigated, as shown in Figure 5b. It is observed that σ increases linearly with $d^{-0.5}$. Through data fitting, the relationship between them is as follows:

$$\sigma = \sigma_0 + k \cdot d^{-\frac{1}{2}} \quad (2)$$

where σ_0 and k are the constants with the values of 1.60 MPa and 135.48 MPa·$\mu m^{1/2}$, respectively.

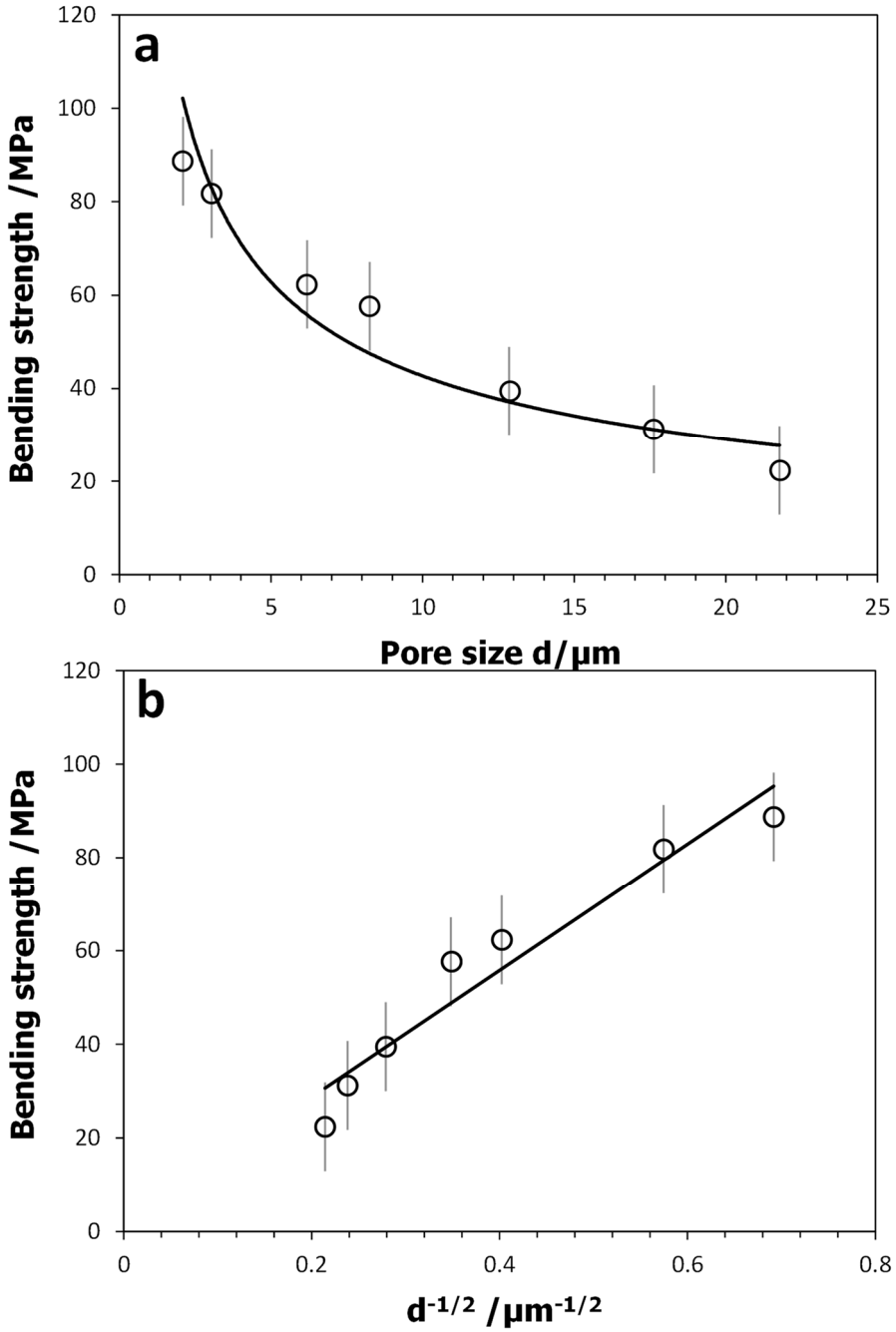

Figure 5. Relationship curves between the bending strength and the average pore size d (**a**) and $d^{-1/2}$ (**b**) for porous Ti_3SiC_2.

The determination coefficient R^2 of the fitting relation equation is 0.94, which shows a higher fitting degree than Equation (1). Equation (2) is the Hall–Petch equation reflecting the relationship between the microstructure parameter and the mechanical property [20,21]. The result indicates that the influence of the pore size on the strength of the reactively synthesized porous Ti_3SiC_2 compound can be described by the Hall–Petch equation under the condition of approximately the same porosities and phase purities. In fact, a similar linear relationship between strength and reciprocal square root of the pore size was also found in porous alumina ceramics [26]. As the main component of the porous material, the pore can be approximately regarded as a phase in composite material. The decrease of pore size weakens the size factor that causes stress concentration [27], which is conducive to the improvement of material strength. On the other hand, the content of MAX phase in the sintered

compacts increases with decreasing the pore size (Figure 2). Compared with Ti_3SiC_2 phase, TiC impurity phase has higher hardness and brittleness. Under the action of external load, this kind of hard and brittle impurity phase can often cause the stress concentration, which results in the decrease of the strength of the material. Therefore, the synthesis of Ti_3SiC_2 phase with high purity has always been the focus of researchers [1,3,25].

In this work, the pore size of porous Ti_3SiC_2 compounds has been adjusted by changing the particle size of TiH_2 powder. In the reactive synthesis process, there is a strict linear relationship between the powder size of TiH_2 and the pore size [6]:

$$d_m = g \cdot d_p \quad (3)$$

where d_m and d_p are the maximum pore size (μm) of porous Ti_3SiC_2 and the powder particle size (μm) of TiH_2, respectively, and g is the proportionality coefficient. Under the same synthetic process conditions, the reduction of powder size is beneficial to obtain the resultant material with smaller pores [6].

Figure 6 shows the relationship between the flexural elastic modulus and the pore size. When the pore size decreases from 21.8 to 2.1 μm, the flexural modulus increases from 13 to 70 GPa, which increases rapidly with the further decrease of the pore size to several microns. For comparison, the Young's and the shear moduli of porous Ti_3SiC_2 with the porosity fraction of ca. 0.5 prepared by space holder were investigated to be about 50 GPa and 20 GPa, respectively [13]. Through data fitting, the relationship between them is as follows:

$$E = h \cdot d^j \quad (4)$$

where E and d are the flexural modulus (GPa) and the average pore size (μm) of porous Ti_3SiC_2, respectively. h and j are the constants with the values of 97.42 and −0.61, respectively.

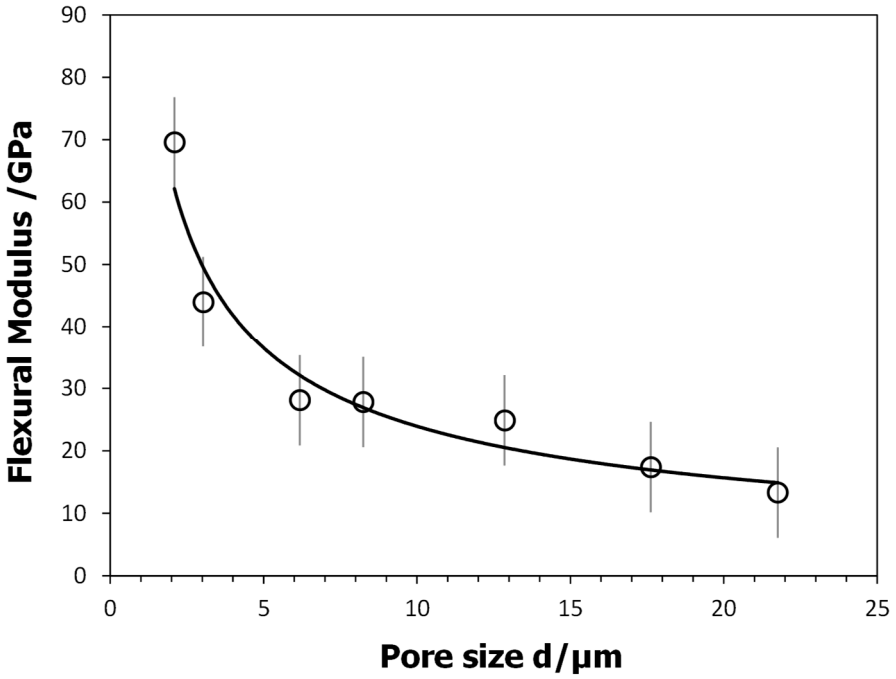

Figure 6. Relation curves between the flexural modulus and the average pore size for porous Ti_3SiC_2.

The determination coefficient R^2 of Equation (4) is 0.95, indicating that the flexural modulus of porous Ti_3SiC_2 has a relatively good power function relation with the pore size. In the investigations on the relation of pore size and elastic modulus for porous materials, there are two kinds of research

results for different material types. On the one hand, it has been revealed that the elastic modulus increases slightly with the increase of the pore size for a porous alumina ceramic [26]. On the other hand, it has been found that the elastic modulus increases with the decrease of the pore size for a porous nickel metal [28]. In this study, the change behavior of Ti_3SiC_2 MAX phase is similar to that of the latter, which indicates that porous Ti_3SiC_2 exhibits similar characteristics to porous metals under the action of bending stress.

4. Conclusions

Reactively synthesized porous Ti_3SiC_2 compounds with different pore sizes have the characteristics of high purity of MAX phase and laminar microstructure. The flexural stress–strain curves of porous Ti_3SiC_2 compounds exhibit two stages of elastic deformation and fracture, and the elastic deformation behavior shows a characteristic of kinking nonlinear elastic solid. The bending strength increases with decreasing the pore size for the synthesized porous Ti_3SiC_2 with approximately the same porosities and phase purities, and the change law between them follows the Hall–Petch equation. The flexural modulus of porous Ti_3SiC_2 has a power function relationship with the pore size. The reduction of the pore size of porous Ti_3SiC_2 improves the phase purity, strength and stiffness while increasing its filtration accuracy.

Author Contributions: Conceptualization, Y.J. and Y.H.; methodology, Y.J.; validation, H.G.; formal analysis, X.L.; investigation, Y.J. and X.L.; resources, Y.J.; data curation, H.G.; writing—original draft preparation, Y.J.; writing—review and editing, Y.J. and Y.H.; supervision, Y.H.; project administration, Y.H.; funding acquisition, Y.J., X.L. and H.G. All authors have read and agreed to the published version of the manuscript.

Funding: This research was funded by the National Natural Science Foundation of China, grant number 51971251, 51774336, 51604305.

Acknowledgments: The work is financially supported by the National Natural Science Foundation of China (No. 51971251, 51774336, 51604305).

Conflicts of Interest: The authors declare no conflict of interest.

References

1. Liu, X.; Zhang, H.; Jiang, Y.; He, Y. Characterization and application of porous Ti_3SiC_2 ceramic prepared through reactive synthesis. *Mater. Des.* **2015**, *79*, 94–98. [CrossRef]
2. Wang, Z.; Jiang, Y.; He, Y. Oxidation behavior of reactively synthesized porous $Ti_3(Si,Al)C_2$ compound at 800 °C in ambient air. *Ceram. Int.* **2019**, *45*, 15482–15487. [CrossRef]
3. Liu, X.; Jiang, Y.; Zhang, H.; Yu, L.; Kang, J.; He, Y. Porous Ti_3SiC_2 fabricated by mixed elemental powders reactive synthesis. *J. Eur. Ceram. Soc.* **2015**, *35*, 1349–1353. [CrossRef]
4. Velasco, B.; Tsipas, S.A.; Ferrari, B.; Gordo, E. MAX phase foams produced via powder metallurgy process using water soluble space holder. *Powder Metall.* **2015**, *58*, 95–99. [CrossRef]
5. Velasco, B.; Gordo, E.; Tsipas, S.A. MAX phase Ti_2AlC foams using a leachable space-holder material. *J. Alloys Compd.* **2015**, *646*, 1036–1042. [CrossRef]
6. Liu, X.; Zhang, H.; Jiang, Y.; He, Y. Factors affecting the property of porous Ti_3SiC_2 metal ceramic fabricated through pressureless sintering. *J. Porous Mater.* **2015**, *22*, 1285–1290. [CrossRef]
7. Wang, Z.; Zhang, H.; Liu, X.; Jiang, Y.; Gao, H.; He, Y. Reactive synthesis of porous nanolaminate $Ti_3(Si,Al)C_2$ intermetallic compound. *Mater. Chem. Phys.* **2018**, *208*, 85–90. [CrossRef]
8. Sun, Z.M.; Murugaiah, A.; Zhen, T.; Zhou, A.; Barsoum, M.W. Microstructure and mechanical properties of porous Ti_3SiC_2. *Acta Mater.* **2005**, *53*, 4359–4366. [CrossRef]
9. Zhao, B.; Gain, A.K.; Ding, W.; Zhang, L.; Li, X.; Fu, Y. A review on metallic porous materials: Pore formation, mechanical properties, and their applications. *Int. J. Adv. Manuf. Technol.* **2018**, *95*, 2641–2659. [CrossRef]
10. Xiong, X.; Wang, Z.; Wang, X.; Liu, H.; Ma, Y. Enhancing the mechanical strength and air permeability of corundum porous materials using shape-modified coarse aggregates. *Ceram. Int.* **2019**, *45*, 11027–11031. [CrossRef]
11. Zhang, B.; Huang, H.; Lu, X. Fabrication and properties of C/SiC porous ceramics by grinding-mould pressing-sintering process. *J. Eur. Ceram. Soc.* **2019**, *39*, 1775–1780. [CrossRef]

12. Zhou, A.G.; Fraczkiewicz, M.; Barsoum, M.W. Mechanical damping in porous Ti_3SiC_2. *Acta Mater.* **2006**, *54*, 5261–5270.
13. Velasco, B.; Gordo, E.; Hu, L.; Radovic, M.; Tsipas, S.A. Influence of porosity on elastic properties of Ti_2AlC and Ti_3SiC_2 MAX phase foams. *J. Alloys Compd.* **2018**, *764*, 24–35. [CrossRef]
14. Finkel, P.; Zhou, A.G.; Basu, S.; Yeheskel, O.; Barsoum, M.W. Direct observation of nonlinear acoustoelastic hysteresis in kinking nonlinear elastic solids. *Appl. Phys. Lett.* **2009**, *94*, 241904. [CrossRef]
15. Zhou, A.G.; Basu, S.; Friedman, G.; Finkel, P.; Yeheskel, O.; Barsoum, M.W. Hysteresis in kinking nonlinear elastic solids and the Preisach-Mayergoyz model. *Phys. Rev. B* **2010**, *82*, 094105. [CrossRef]
16. Liu, X.; Zhang, Q.; Zhang, H.; Jiang, Y.; He, Y. Development and characterization of microporous Ti_3SiC_2 ceramic membranes for filtration of microorganisms. *J. Mater. Sci.* **2016**, *51*, 2594–2597. [CrossRef]
17. Gao, H.Y.; He, Y.H.; Zou, J.; Shen, P.Z.; Jiang, Y.; Liu, C.T. Mechanical properties of porous Fe-Al intermetallics. *Powder Metall.* **2015**, *58*, 197–201. [CrossRef]
18. Liu, G.; Lu, D.H.; Liu, X.W.; Liu, F.C.; Yang, Q.; Du, H.; Hu, Q.; Fan, Z.T. Solute segregation effect on grain boundary migration and Hall–Petch relationship in CrMnFeCoNi high-entropy alloy. *Mater. Sci. Technol.* **2019**, *35*, 500–508. [CrossRef]
19. Ryou, H.; Drazin, J.W.; Wahl, K.J.; Qadri, S.B.; Gorzkowski, E.P.; Feigelson, B.N.; Wollmershauser, J.A. Below the hall–petch limit in nanocrystalline ceramics. *ACS Nano* **2018**, *12*, 3083–3094. [CrossRef]
20. Wollmershauser, J.A.; Feigelson, B.N.; Gorzkowski, E.P.; Ellis, C.T.; Goswami, R.; Qadri, S.B.; Tischler, J.G.; Kub, F.J.; Everett, R.K. An extended hardness limit in bulk nanoceramics. *Acta Mater.* **2014**, *69*, 9–16. [CrossRef]
21. Wang, C.; Jiang, C.; Cai, F.; Zhao, Y.; Zhu, K.; Chai, Z. Effect of shot peening on the residual stresses and microstructure of tungsten cemented carbide. *Mater. Des.* **2016**, *95*, 159–164. [CrossRef]
22. Roa, J.J.; Jiménez-Piqué, E.; Tarragó, J.M.; Sandoval, D.A.; Mateo, A.; Fair, J.; Llanes, L. Hall–Petch strengthening of the constrained metallic binder in WC–Co cemented carbides: Experimental assessment by means of massive nanoindentation and statistical analysis. *Mater. Sci. Eng. A* **2016**, *676*, 487–491. [CrossRef]
23. Li, C.L.; Mei, Q.S.; Li, J.Y.; Chen, F.; Ma, Y.; Mei, X.M. Hall–Petch relations and strengthening of Al-ZnO composites in view of grain size relative to interparticle spacing. *Scr. Mater.* **2018**, *153*, 27–30. [CrossRef]
24. He, W.; Weng, Q.G.; He, Y.H.; Jiang, Y. Preparation of ultrafine Ti powder by inhibitor coated/HDH combined method. *Powder Metall.* **2013**, *56*, 239–244. [CrossRef]
25. Zhang, Z.F.; Sun, Z.M.; Hashimoto, H. Rapid synthesis of ternary carbide Ti_3SiC_2 through pulse-discharge sintering technique from Ti/Si/TiC powders. *Metall. Mater. Trans. A* **2002**, *33*, 3321–3328. [CrossRef]
26. Ashizuka, M.; Ishida, E.; Matsushita, T.; Hisanaga, M. Elastic modulus, strength and fracture toughness of alumina ceramics containing pores. *J. Ceram. Soc. Jpn.* **2002**, *110*, 554–559. [CrossRef]
27. Xu, Z.; Wen, W.; Zhai, T. Effects of pore position in depth on stress/strain concentration and fatigue crack initiation. *Metall. Mater. Trans. A* **2012**, *43*, 2763–2770. [CrossRef]
28. Li, Z.; Yang, L.; Li, Y.; Yang, Y.; Zhou, C.; Ding, Y.; Zhao, J.; Li, Y. Effects of pore size on the mechanical properties of three-dimensionally ordered macroporous nickel. *Mater. Des.* **2013**, *45*, 52–55. [CrossRef]